GSA Data Repository 2016347

Paleo-Asian Oceanic slab under the North China Craton revealed by carbonatites derived from subducted limestones

Chunfei Chen[1], Yongsheng Liu[1*], Stephen F. Foley[2], Mihai N. Ducea[3,4], Detao He[1], Zhaochu Hu[1], Wei Chen[1], Keqing Zong[1]

[1] *State Key Laboratory of Geological Processes and Mineral Resources, School of Earth Sciences, China University of Geosciences, Wuhan 430074, China*

[2]*ARC Centre of Excellence for Core to Crust Fluid Systems, Dept. of Earth and Planetary Sciences, Macquarie University, North Ryde, New South Wales 2109, Australia.*

[3] *Department of Geosciences, University of Arizona, Tucson, AZ 85721, USA*
[4] *Faculty of Geology and Geophysics, University of Bucharest, Bucharest, Romania*

Analytical methods

Whole rock samples were crushed in a corundum jaw crusher, and the resulting chips were handpicked to exclude the olivine, pyroxene and spinel xenocrysts. About 100g of the sample was then powdered in an agate ring mill to less than 200 mesh.

The sample powders were digested by HF + HNO_3 in Teflon bombs and analyzed using an Agilent 7500a ICP-MS at the State Key Laboratory of Geological Processes and Mineral Resources, China University of Geosciences, Wuhan (SKL GPMR-CUG). The detailed sample digestion procedure for ICP-MS analysis is given in Liu et al. (2008a). Analyses of rock standards (BCR-2, BHVO-2 and AGV-2) indicate accuracies are better than 5% for major elements and 10% for trace elements.

The selected samples were leached using 1N acetic acid to dissolve carbonate for Sr and Nd isotopic analyses. The leachate is believed to be the bulk carbonate component in the carbonatite. The chemical separation for Sr and Nd isotopic analyses is the same as the description by Gao et al. (2004). Sr-Nd isotopic ratios were determined using a Triton Ti TIMS at the SKL GPMR-CUG. The measured $^{143}Nd/^{144}Nd$ and $^{87}Sr/^{86}Sr$ ratios were normalized to $^{146}Nd/^{144}Nd$ =0.7219 and $^{88}Sr/^{86}Sr$ = 8.375209, respectively. BCR-2 and GBW04411 were used as the monitor standard materials in this work. Our analytical results ($^{143}Nd/^{144}Nd$ = 0.512629 ± 0.000006 (2σ) for BCR-2 and $^{87}Sr/^{86}Sr$ = 0.760033 ± 0.000016(2σ) for GBW04411) fit the recommend values ($^{143}Nd/^{144}Nd$ =0.512636±0.000002 (2SD) for BCR-2; $^{87}Sr/^{86}Sr$ =0.76±0.000006 (2SD) for GBW04411) within

analytical uncertainty.

Major and trace elements of silicate minerals, carbonate matrix and phenocrysts were analyzed by LA-ICP-MS with a spot size of 44 μm at the SKL GPMR-CUG. Element contents were calibrated against multiple reference materials without applying internal standardization. Details of operating conditions for LA-ICP-MS and data reduction strategy are same as Liu et al. (2008b) for silicate minerals and Chen et al. (2011) for carbonate. Off-line selection and integration of the background and the analyzed signals, along with time-drift correction and quantitative calibration, were performed by ICPMSDataCal (Liu et al., 2008b).

The polished sections were prepared for identifying moissanite and highly disordered graphite using a Thermo Scientific DRX dispersive Raman micro-spectrometer. In order to avoid possible contamination, Al_2O_3 abrasive papers only were used to prepare the polished sections. The detailed sample preparation procedure is given in Liu et al. (2015).

Data sources for carbonatite and limestone

Carbonatites are compiled from a worldwide database (Bühn, 2008; Bell et al., 1982; Bell and Simonetti, 2010; Halama et al., 2008; Hoernle et al., 2002; Hou et al., 2015; Huang et al., 1995; Mitchell, 2005; Mourao et al., 2010).

Major elements in limestone were collected from worldwide (Armstrong-Altrin et al., 2003; Bellanca et al., 1997; Jin et al., 2009; Klein and Beukes, 1989; Tanaka et al., 2003; Tsikos et al., 2001). Trace elements in limestone collected from worldwide (Bellanca et al., 1997; Jin et al., 2009; Tanaka et al., 2003; Tsikos et al., 2001) are shown for comparison.

Detailed explanation, data sources and modelling parameters for Fig. 3

The CaO versus Ni plot in Fig.3 (A) shows that the carbonates in the carbonatite intrusion trend to high Ni contents, in contrast to limestones. The solid curve is a simple mixing line between limestone and the Hannuoba peridotite (Rudnick et al., 2004): ticks on curves show 10% increments. Average of peridotites from Hannuoba (Rudnick et al., 2004) is shown for comparison. (B) Sr-Nd isotopic compositions of the Hannuoba intrusion (this paper). Aragonite veinlets (this paper), limestone (Keto and Jacobsen, 1988; Veizer et al., 1999), typical carbonatites (Bühn, 2008; Bell et al., 1982; Bell and Simonetti, 2010; Halama et al., 2008; Hoernle et al., 2002; Hou et al., 2015; Huang et al., 1995; Mitchell, 2005; Mourao et al., 2010), the Mesozoic carbonatites from Zhuolu (ZL) and Huairen (HR) (Yan et al., 2007), peridotite and garnet pyroxenite xenoliths (Rudnick et al., 2004; Xu, 2002), and alkali basalt (Song et al., 1990) from Hannuoba are shown for comparison. Average Sr and Nd contents (Sr=380 ppm; Nd=0.66 ppm) in Silurian, Devonian and Carboniferous limestones from the Inner Mongolia derived from the Paleo-Asian Ocean (Liu, et al. unpublished data) were used in model calculations. Detailed parameters are listed in the table below.

The trend to high Ni contents shown by the carbonates could reflect mixing in of a lower proportion of peridotite (~10%) (Fig. 3A) than that of the trend to high $^{143}Nd/^{144}Nd$ (~30%) (Fig. 3B). This could be attributed to the transfer of Ni from carbonatite melt to newly growth silicate minerals (i.e. clinopyroxene) during carbonatite-peridotite interaction.

Compositional parameters	Sr	Nd
Limestone (ppm)	380	0.66
Limestone isotope ratios	0.707-0.709	0.5119-0.5123
Average of Hannuoba peridotites (ppm)	14.6	1.09
Average of Hannuoba peridotites isotopic ratios	0.7038	0.51310

Figure DR1

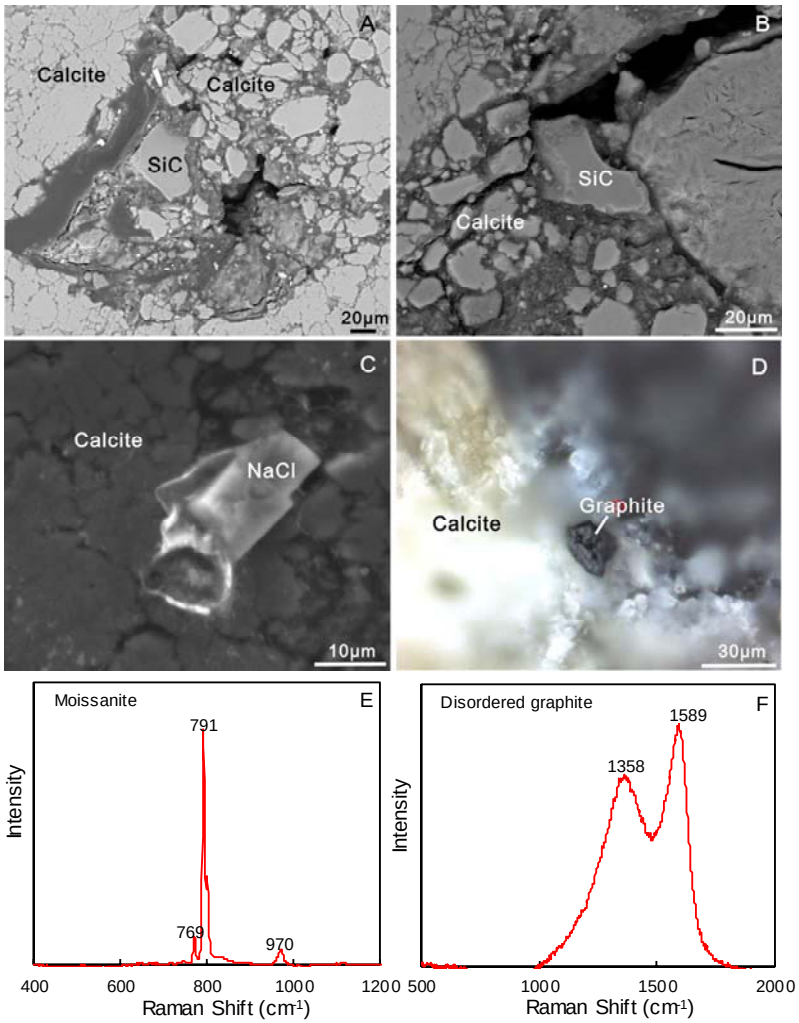

Moissanite (A and B), Na chloride (C) and graphite (D) coexisting with carbonate in the carbonatite intrusion. Raman shift of moissanite (E) and highly disordered graphite (F) in the carbonatite intrusion.

Figure DR2

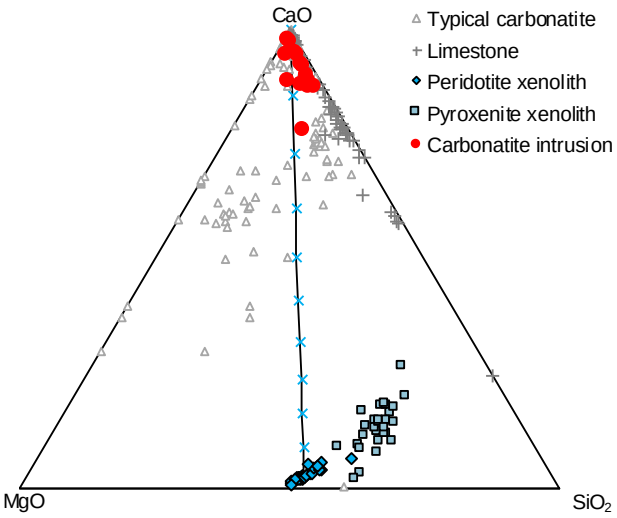

CaO-MgO-SiO_2 diagram of the Hannuoba carbonatite intrusion (red circles). The solid line with crosses is a mixing line showing 10% increments between pure limestone and peridotite. Peridotite xenoliths (Rudnick et al., 2004) and pyroxenite veins (Liu et al., 2005; Xu, 2002) in peridotite xenoliths from Hannuoba, limestone (Armstrong-Altrin et al., 2003; Bellanca et al., 1997; Jin et al., 2009; Klein and Beukes, 1989; Tanaka et al., 2003; Tsikos et al., 2001) and typical carbonatites (Bühn, 2008; Bell et al., 1982; Bell and Simonetti, 2010; Halama et al., 2008; Hoernle et al., 2002; Hou et al., 2015; Huang et al., 1995; Mitchell, 2005; Mourao et al., 2010) are shown for comparison.

Figure DR3

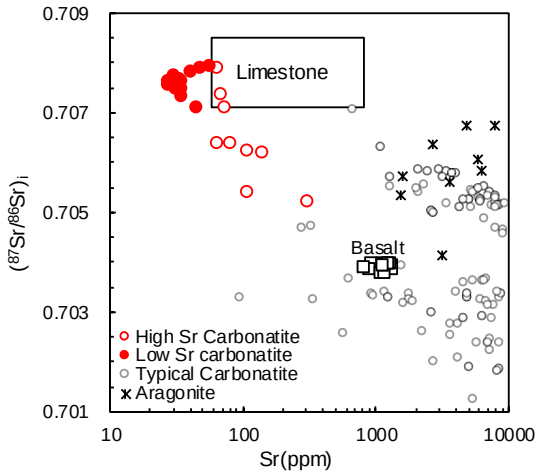

Variations of $(^{87}Sr/^{86}Sr)_I$ with Sr contents for carbonates and aragonite veins in the Hannuoba carbonatite intrusion. The carbonatite intrusion can be classified into two types: low Sr carbonatite (Sr 30~50 ppm) and high Sr carbonatite (Sr >60 ppm). The isotopic compositions are calculated back to 22 Ma (age of the Hannuoba basalt). The typical carbonatites (data sources as in Figure DR2) and alkali basalts from Hannuoba are shown for comparison. Sr isotopic data for limestone are from Veizer et al. (1999).

Figure DR4

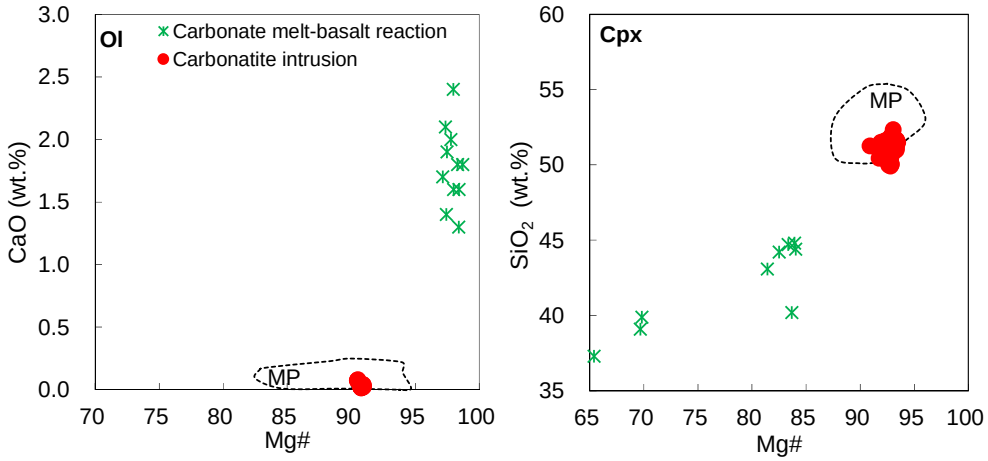

Plots of Mg# versus CaO and SiO_2 for Ol and Cpx xenocrysts from the Hannuoba carbonatite intrusion, eliminating the possibility that the carbonatite composition could be due to interaction between carbonate and basaltic melt. Data for Ol and Cpx formed by carbonate melt-basalt interaction are from Jolis et al. (2013). MP = Range of mantle peridotites from the North China Craton (e.g., Rudnick et al., 2004; Xu et al., 2013).

Figure DR5

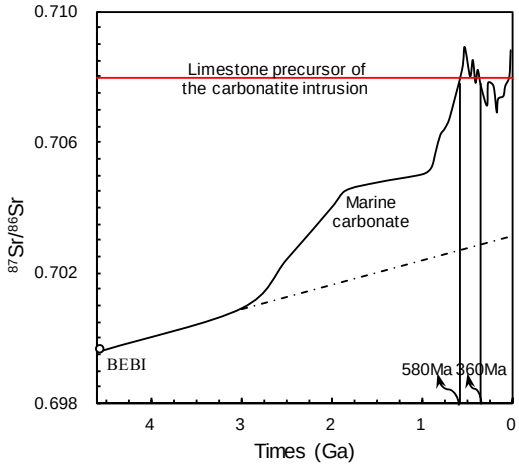

($^{87}Sr/\ ^{86}Sr)_I$ comparison between the limestone precursor of the Hannuoba carbonatite and the evolution line of marine carbonates (Veizer, 1985; Veizer et al., 1999). The intersection points infer that the limestone precursor of the carbonatite intrusion was certainly not older than 580 Ma, and most probably between 360 and 580 Ma. BEBI = Bulk-Earth best initial.

References not cited in main paper

The temperatures of silicate macrocrysts were estimated using thermometer of Cpx + Opx pairs (Wells, 1977).

(Burke et al., 2003)

Table DR 1

Compositions of silicate mineral xenocrysts in the Hannuoba carbonatite intrusion
Units are wt.% for major elements and ppm for Ni.

Num.	JSB011		JSB029			JSB012		JSB024			JSB044		JSB054	
	Cpx	Opx	Cpx	Ol	Opx	Cpx	Opx	Cpx	Opx	Ol	Cpx	Opx	Cpx	Opx
SiO_2	51.2	54.8	50.8	39.0	54.5	50.1	55.4	51.3	55.4	39.5	50.6	54.3	51.1	55.7
TiO_2	0.30	0.08	0.11	0.00	0.04	0.33	0.07	0.29	0.08	0.00	0.32	0.08	0.34	0.08
Al_2O_3	5.18	3.79	4.40	0.03	4.04	5.88	3.46	5.00	3.35	0.01	5.75	4.15	4.69	3.47
TFeO	2.36	5.27	2.68	9.15	5.97	2.21	6.11	2.07	5.70	9.12	2.25	5.59	2.70	5.76
MnO	0.08	0.13	0.09	0.14	0.14	0.07	0.14	0.08	0.14	0.13	0.08	0.13	0.08	0.14
MgO	16.7	34.6	17.7	51.2	33.5	15.9	33.8	16.3	34.1	50.7	16.2	34.3	17.2	33.5
CaO	21.6	0.65	22.5	0.08	0.98	22.9	0.46	22.3	0.51	0.03	21.9	0.61	21.3	0.62
Na_2O	1.39	0.08	0.62		0.05	1.44	0.05	1.34	0.06		1.54	0.07	1.32	0.1
K_2O	0.00	0.00	0.01	0.00	0.00	0.00	0.00	0.00	0.00	0.00	0.00	0.00	0.01	0.00
P_2O_5	0.01	0.01	0.01	0.02	0.01	0.01	0.01	0.01	0.01	0.01	0.01	0.01	0.02	0.01
Mg#	92.6	92.1	92.2	90.9	90.9	92.8	90.8	93.3	91.4	90.8	92.8	91.6	91.9	91.2
Ni	348	734	376	2809	809	287	691	308	713	3062	327	715	378	755

Table DR 2

Major and trace element, Sr-Nd isotopic and C-O isotopic compositions of carbonate components in carbonatite intrusion. Units are wt.% for major elements, ppm for trace elements and ‰ for C-O isotopes.

	Carbonatite intrusion (JSB-)										
Num.	12011	12022	12023	12029	12032	12033	12044	12046	12049	12051	12053
SiO_2	5.04	3.12	3.33	5.31	2.05	4.48	4.91	4.44	0.31	1.88	6.32
TiO_2	0.008	0.004	0.029	0.012	0.006	0.003	0.012	0.013	0.006	0.003	0.012
Al_2O_3	0.73	0.51	0.60	0.42	0.40	0.59	1.24	1.45	0.42	0.66	1.19
FeO	1.41	1.03	1.57	1.63	1.32	1.55	1.11	1.30	1.17	1.04	1.28
MgO	1.39	0.90	1.04	1.58	0.88	1.08	1.35	2.18	0.80	0.85	1.59
CaO	50.1	52.3	51.4	49.7	52.7	50.8	50.2	49.2	53.9	52.9	49.0
Na_2O	0.007	0.013	0.006	0.016	0.01	0.008	0.008	0.014	0.005	0.009	0.013
K_2O	0.019	0.014	0.02	0.023	0.014	0.017	0.014	0.016	0.012	0.026	0.016
Sc	1.02	0.40	0.97	2.25	0.89	0.80	0.69	0.65	0.36	0.29	0.80
V	2.68	1.94	2.73	2.36	1.70	3.25	2.23	3.36	1.11	1.38	2.60
Cr	61.5	35.4	56.4	104	91.5	285	16.5	57.8	8.47	2.39	125
Co	4.02	1.22	3.50	6.11	2.63	3.60	1.10	7.35	3.46	1.48	10.0
Ni	113	58.3	118	169	98.6	113	74.4	181	132	96.7	145
Rb	0.69	0.25	0.67	0.41	0.24	0.58	0.29	0.38	0.27	0.65	0.41
Sr	32.4	27.5	30.6	34.2	29.8	34.3	31.7	55.7	34.1	47.0	79.1
Y	1.72	1.20	1.29	1.68	1.16	0.87	2.30	0.53	0.56	0.55	0.50
Zr	2.04	0.70	4.04	1.71	0.65	0.65	2.91	2.88	1.60	1.68	1.71
Nb	0.21	0.15	0.77	0.39	0.18	0.10	0.34	0.55	0.20	0.36	0.41
Ba	0.44	0.39	0.35	0.82	0.16	0.28	0.35	1.26	0.35	1.07	1.48
La	1.44	1.66	1.48	1.56	1.53	1.10	2.36	0.56	0.57	0.88	0.48
Ce	1.34	1.73	2.24	2.16	1.91	0.83	3.54	0.67	0.58	0.69	0.63
Pr	0.37	0.27	0.31	0.39	0.27	0.15	0.62	0.11	0.11	0.12	0.095
Nd	1.73	1.16	1.43	1.79	1.12	0.69	2.85	0.49	0.46	0.48	0.43
Sm	0.43	0.22	0.35	0.42	0.23	0.14	0.73	0.099	0.10	0.10	0.089
Eu	0.25	0.12	0.13	0.20	0.12	0.089	0.32	0.049	0.056	0.042	0.034
Gd	0.41	0.23	0.28	0.40	0.26	0.15	0.60	0.11	0.10	0.098	0.079
Tb	0.07	0.03	0.04	0.06	0.03	0.02	0.08	0.01	0.01	0.01	0.01
Dy	0.36	0.14	0.22	0.30	0.14	0.11	0.43	0.081	0.080	0.059	0.078
Ho	0.07	0.03	0.04	0.05	0.03	0.02	0.08	0.01	0.02	0.01	0.02
Er	0.17	0.063	0.094	0.12	0.071	0.050	0.19	0.036	0.040	0.029	0.034
Tm	0.028	0.008	0.011	0.019	0.009	0.006	0.024	0.005	0.005	0.004	0.004
Yb	0.15	0.045	0.081	0.12	0.056	0.044	0.13	0.027	0.036	0.025	0.035
Lu	0.023	0.008	0.011	0.018	0.009	0.005	0.019	0.005	0.004	0.005	0.005
Hf	0.021	0.009	0.078	0.029	0.014	0.007	0.036	0.041	0.016	0.019	0.027
Ta	0.013	0.010	0.044	0.021	0.013	0.010	0.020	0.026	0.012	0.009	0.020
Pb	0.10	0.051	0.12	0.39	0.11	0.076	0.094	0.13	0.080	0.10	0.10
Th	0.02	0.01	0.06	0.03	0.01	0.01	0.02	0.02	0.01	0.03	0.02
U	0.15	0.087	0.11	0.12	0.11	0.15	0.17	0.34	0.15	0.29	0.24
Ce/Ce*	0.45	0.63	0.80	0.68	0.72	0.50	0.71	0.66	0.56	0.51	0.71
Eu/Eu*	1.78	1.62	1.17	1.50	1.42	1.80	1.44	1.40	1.62	1.27	1.21
$^{87}Rb/^{86}Sr$	0.0598	0.0256	0.0621	0.0338	0.0223	0.0476	0.0258	0.0192	0.0222	0.0387	0.0145
$^{87}Sr/^{86}Sr$	0.707496	0.707576	0.707780	0.707343	0.707710	0.707640	0.707509	0.707963	0.707509	0.707902	0.706383
2σ	4	5	5	6	5	7	5	5	17	18	5
$^{147}Sm/^{144}Nd$	0.1564	0.1218	0.1539	0.1479	0.1308	0.1321	0.1600	0.1274	0.1427	0.1306	0.1293
$^{143}Nd/^{144}Nd$	0.512869	0.512884	0.512866	0.512887	0.51291	0.512885	0.512909	0.512894	0.512941	0.512872	0.512874
2σ	5	4	8	4	4	9	4	7	16	12	13
$\delta^{13}C_{VPDB}$	-12.0	-12.4	-12.6	-13.1	-11.9	-12.1	-11.9	-11.4	-12.8	-11.3	-12.2
$\delta^{18}O_{SMOW}$	22.7	22.8	22.6	22.6	22.8	22.8	22.7	22.7	22.5	22.6	22.3

Table DR 2 continued

	Carbonatite intrusion (JSB-)									
Num.	12055	12057	12058	12061	12063	12093	14005	14035	14045	14009
SiO_2	7.55	2.20	0.92	5.91	2.59	3.76	7.36	3.68	16.00	2.70
TiO_2	0.026	0.011	0.023	0.008	0.009	0.003	0.016	0.008	0.008	0.005
Al_2O_3	1.76	0.55	1.16	0.80	0.86	0.44	1.86	0.42	0.51	1.37
FeO	1.27	1.13	1.64	1.13	0.91	1.17	1.28	1.45	0.52	0.73
MgO	3.00	1.18	2.03	1.10	1.43	1.24	4.81	1.56	2.03	3.35
CaO	46.4	52.3	51.2	50.2	51.8	51.4	44.2	50.8	44.1	49.4
Na_2O	0.012	0.005	0.012	0.006	0.009	0.006	0.03	0.009	0.011	0.014
K_2O	0.015	0.013	0.02	0.013	0.024	0.014	0.012	0.012	0.039	0.013
Sc	0.70	0.37	0.95	0.42	0.40	0.52	1.57	0.80	0.36	0.40
V	3.10	1.63	3.51	1.25	1.58	1.47	7.08	3.41	1.70	1.70
Cr	56.2	11.0	84.2	21.6	1.48	9.75	181	112	13.6	21.7
Co	5.17	4.33	6.01	2.72	1.79	1.79	8.75	3.00	1.74	1.51
Ni	127	129	198	119	93.3	94.1	208	152	156	83.9
Rb	0.41	0.30	0.45	0.27	0.74	0.43	0.19	0.32	2.84	0.22
Sr	109	106	40.1	33.8	306	68.7	64.7	72.9	138	63.3
Y	1.82	0.69	0.94	0.62	0.62	3.26	1.83	0.86	0.45	0.72
Zr	6.76	2.02	2.92	1.77	3.98	1.45	1.26	1.30	1.67	0.54
Nb	1.06	0.34	0.63	0.31	0.78	0.10	0.22	0.17	0.31	0.21
Ba	1.45	0.44	0.86	0.39	1.71	1.71	0.92	1.01	1.07	0.67
La	2.46	0.93	1.03	0.73	0.89	2.31	1.39	0.72	0.81	1.15
Ce	2.82	1.09	1.58	0.96	1.07	0.55	0.45	0.56	0.57	0.95
Pr	0.41	0.15	0.23	0.14	0.15	0.31	0.23	0.10	0.11	0.15
Nd	1.73	0.67	0.97	0.67	0.65	1.38	1.06	0.46	0.40	0.58
Sm	0.38	0.15	0.24	0.16	0.12	0.25	0.28	0.11	0.087	0.11
Eu	0.26	0.074	0.088	0.067	0.076	0.12	0.13	0.045	0.080	0.044
Gd	0.38	0.14	0.22	0.15	0.14	0.37	0.30	0.12	0.072	0.11
Tb	0.048	0.022	0.031	0.021	0.019	0.043	0.042	0.017	0.011	0.014
Dy	0.27	0.098	0.16	0.12	0.12	0.26	0.26	0.099	0.066	0.081
Ho	0.050	0.019	0.028	0.018	0.019	0.056	0.045	0.021	0.013	0.016
Er	0.13	0.047	0.076	0.050	0.040	0.16	0.13	0.051	0.040	0.040
Tm	0.019	0.007	0.010	0.005	0.007	0.023	0.017	0.007	0.007	0.0057
Yb	0.12	0.045	0.055	0.040	0.038	0.14	0.11	0.044	0.041	0.030
Lu	0.016	0.005	0.010	0.006	0.006	0.023	0.018	0.007	0.008	0.006
Hf	0.073	0.033	0.053	0.029	0.037	0.009	0.027	0.017	0.024	0.010
Ta	0.046	0.018	0.038	0.014	0.019	0.008	0.013	0.010	0.024	0.028
Pb	0.12	0.082	0.16	0.066	0.22	0.11	0.063	0.088	0.22	0.082
Th	0.043	0.020	0.078	0.013	0.059	0.015	0.013	0.008	0.027	0.007
U	0.29	0.11	0.13	0.16	0.44	0.19	0.19	0.20	0.32	0.18
Ce/Ce*	0.68	0.71	0.79	0.71	0.71	0.16	0.19	0.51	0.46	0.56
Eu/Eu*	2.07	1.51	1.15	1.29	1.82	1.23	1.33	1.15	2.98	1.19
$^{87}Rb/^{86}Sr$	0.0105	0.0079	0.0313	0.0224	0.0069	0.0177	0.0082	0.0125	0.0578	0.0098
$^{87}Sr/^{86}Sr$	0.706225	0.705401	0.707822	0.707681	0.705222	0.707374	0.707908	0.707108	0.706217	0.706388
2σ	6	5	5	6	5	6	5	5	14	10
$^{147}Sm/^{144}Nd$	0.1394	0.1413	0.1554	0.1459	0.1141	0.1145	0.1644	0.1562	0.1351	0.1214
$^{143}Nd/^{144}Nd$	0.512906	0.512912	0.5129	0.512903	0.512902	0.512871	0.512918	0.512862	0.512817	0.512976
2σ	6	4	5	4	6	5	7	14	6	23
$\delta^{13}C_{VPDB}$	-12.7	-14.4	-13.5	-13.3	-13.6	-11.3	-11.9	-11.8	-11.4	-11.2
$\delta^{18}O_{SMOW}$	22.2	22.6	22.6	22.6	22.6	23.0	22.6	22.5	22.6	23.0

Based on the normalization strategy of bulk components as 100%, SiO_2^* is calculated by 100%-the sum of all other major element concentrations expressed as carbonates.

Table DR 3

Compositions of calcite phenocryst (CP) and calcite matrix (CM) in the Hannuoba carbonatite intrusion. Units are wt.% for major elements and ppm for Ni.

Sample Name		CaO	MgO	FeO	SiO_2	Al_2O_3	Ni
JSB011-Cc1-01	CP	55.3	0.23	0.08	0.20	0.00	6.8
JSB011-Cc1-02	CP	55.5	0.20	0.05	0.18	0.00	1.6
JSB011-Cc1-03	CP	55.4	0.22	0.04	0.26	0.00	1.4
JSB012-Cc1-01	CP	53.8	0.58	0.18	0.91	0.01	49.2
JSB012-Cc1-02	CP	54.5	0.48	0.10	0.61	0.00	34.4
JSB012-Cc1-03	CP	54.4	0.61	0.08	0.50	0.00	39.4
JSB012-Cc2-01	CP	54.7	0.60	0.03	0.44	0.00	2.7
JSB012-Cc2-02	CP	54.6	0.68	0.03	0.40	0.00	3.2
JSB012-Cc2-03	CP	54.8	0.59	0.03	0.34	0.00	3.3
JSB024-Cc1-01	CP	53.7	1.42	0.06	0.36	0.00	3.9
JSB024-Cc1-02	CP	53.5	1.62	0.06	0.41	0.00	3.4
JSB024-Cc1-03	CP	53.9	1.33	0.08	0.28	0.00	1.5
JSB024-Cc2-01	CP	54.5	0.63	0.07	0.49	0.01	9.3
JSB024-Cc2-02	CP	54.5	0.45	0.13	0.58	0.02	13.2
JSB024-Cc2-03	CP	54.9	0.36	0.07	0.42	0.01	8.0
JSB029-Cc1-01	CP	53.6	1.63	0.08	0.28	0.00	1.5
JSB029-Cc1-02	CP	53.6	1.59	0.09	0.31	0.00	1.8
JSB029-Cc1-03	CP	53.2	1.65	0.12	0.50	0.02	10.3
JSB029-Cc2-01	CP	54.2	0.58	0.12	0.64	0.03	11.7
JSB029-Cc2-02	CP	48.9	1.04	0.98	3.30	0.21	98.9
JSB044-Cc1-04	CP	53.7	1.61	0.02	0.30	0.00	5.6
JSB044-Cc1-05	CP	53.9	1.54	0.02	0.21	0.00	4.9
JSB044-Cc1-06	CP	53.6	1.74	0.02	0.23	0.00	4.9
JSB044-Cc2-03	CP	54.8	0.26	0.09	0.53	0.04	8.0
JSB044-Cc2-04	CP	54.9	0.39	0.08	0.40	0.03	7.9
JSB044-Cc2-05	CP	51.6	0.46	0.50	1.99	0.40	41.8
JSB044-Cc2-06	CP	54.2	0.26	0.20	0.81	0.13	15.0
JSB054-Cc1-01	CP	54.7	0.30	0.06	0.48	0.08	7.9
JSB054-Cc1-02	CP	54.9	0.47	0.03	0.33	0.01	4.4
JSB054-Cc3-05	CP	54.0	0.43	0.18	0.84	0.05	19.7
JSB054-Cc3-06	CP	54.4	0.53	0.12	0.55	0.03	17.0
JSB054-Cc3-07	CP	52.8	0.44	0.42	1.39	0.17	37.9
JSB054-Cc3-08	CP	53.6	0.31	0.24	1.07	0.16	26.9
JSB054-Cc3-09	CP	55.2	0.31	0.03	0.30	0.00	4.4
JSB054-Cc3-10	CP	54.4	0.39	0.16	0.70	0.04	18.0
JSB057-Cc3-02	CP	55.2	0.19	0.07	0.32	0.00	5.1
JSB057-Cc3-03	CP	55.3	0.20	0.06	0.29	0.00	5.4
JSB057-Cc1-01	CP	52.0	0.53	0.53	1.79	0.16	65.8
JSB057-Cc1-02	CP	52.6	0.40	0.43	1.59	0.19	55.7
JSB057-Cc1-03	CP	53.7	0.32	0.31	1.05	0.07	38.1
JSB057-Cc1-04	CP	50.8	0.45	0.72	2.54	0.34	88.6

Table DR 3 continued

Sample Name		CaO	MgO	FeO	SiO_2	Al_2O_3	Ni
JSB011-Cc2-01	CM	51.2	0.48	0.94	2.31	0.11	36.8
JSB011-Cc2-02	CM	51.1	0.48	0.98	2.27	0.14	36.1
JSB011-Cc2-03	CM	52.7	0.41	0.58	1.54	0.08	21.7
JSB011-Cc2-04	CM	52.1	0.48	0.74	1.78	0.08	24.7
JSB024-Cc3-01	CM	51.6	0.54	0.79	2.06	0.05	36.0
JSB024-Cc3-02	CM	49.8	0.69	1.15	2.97	0.08	62.9
JSB024-Cc3-03	CM	50.3	0.69	1.06	2.74	0.06	57.5
JSB024-Cc3-04	CM	48.8	0.72	1.27	3.53	0.14	104
JSB024-Cc3-05	CM	49.8	0.62	1.07	3.10	0.11	101
JSB029-Cc1-01	CM	48.0	1.03	1.57	3.74	0.08	55.9
JSB029-Cc1-02	CM	46.8	1.20	1.85	4.30	0.06	54.2
JSB044-Cc1-01	CM	51.0	0.47	0.88	2.37	0.23	29.1
JSB044-Cc1-02	CM	47.1	0.90	1.49	4.12	0.49	68.3
JSB044-Cc1-03	CM	46.2	0.91	1.81	4.63	0.43	133
JSB044-Cc1-07	CM	51.5	0.53	0.82	2.00	0.18	44.7
JSB044-Cc1-08	CM	51.6	0.51	0.79	2.03	0.16	38.4
JSB044-Cc2-01	CM	51.1	0.60	0.85	2.24	0.22	34.7
JSB044-Cc2-02	CM	48.4	0.66	1.56	3.64	0.23	56.2
JSB054-Cc3-01	CM	47.5	0.74	1.07	4.00	0.82	80.5
JSB054-Cc3-02	CM	49.8	0.63	0.79	2.91	0.50	62.9
JSB054-Cc3-03	CM	49.7	0.60	0.77	2.99	0.50	63.2
JSB054-Cc3-04	CM	51.1	0.52	0.74	2.33	0.26	50.0
JSB057-Cc3-01	CM	52.5	0.47	0.60	1.65	0.02	35.8
JSB057-Cc3-04	CM	50.8	0.62	0.93	2.48	0.04	80.5
JSB054-Cc1-03	CM	49.6	1.11	0.69	2.89	0.31	76.5
JSB054-Cc1-04	CM	45.2	1.80	0.87	4.97	0.70	116

Table DR 4

Sr content and Sr isotopic compositions of aragonite veinlets crosscutting one sample of the carbonatite intrusion.

Sample	Sr (ppm)	$^{87}Sr/^{86}Sr$	2σ
JSB15062-1	6022	0.70605	0.000015
JSB15062-2	1610	0.70571	0.000039
JSB15062-3	2700	0.70635	0.000034
JSB15062-4	4909	0.70673	0.000016
JSB15062-5	7848	0.70672	0.000013
JSB15062-6	3654	0.70560	0.000019
JSB15062-7	1545	0.70532	0.000047
JSB15062-8	6442	0.70583	0.000027
JSB15062-9	5005	0.70683	0.000017
JSB15062-10	5005	0.70684	0.000021
JSB15062-11	4941	0.70584	0.000030
JSB15062-13	3246	0.70411	0.000039

References

Armstrong-Altrin, J. S., Verma, S. P., Madhavaraju, J., Lee, Y. I., and Ramasamy, S., 2003, Geochemistry of Upper Miocene Kudankulam Limestones, Southern India: International Geology Review, v. 45, p. 16-26, doi: 10.2747/0020-6814.45.1.16.

Bühn, B., 2008, The role of the volatile phase for REE and Y fractionation in low-silica carbonate magmas: implications from natural carbonatites, Namibia: Mineralogy and Petrology, v. 92, p. 453-470, doi: 10.1007/s00710-007-0214-4.

Bell, K., Blenkinsop, J., Cole, T. J. S., and Menagh, D. P., 1982, Evidence from Sr isotopes for long-lived heterogeneities in the upper mantle: Nature, v. 298, p. 251-253, doi: 10.1038/298251a0.

Bell, K., and Simonetti, A., 2010, Source of parental melts to carbonatites–critical isotopic constraints: Mineralogy and Petrology, v. 98, p. 77-89, doi: 10.1007/s00710-009-0059-0.

Bellanca, A., Masetti, D., and Neri, R., 1997, Rare earth elements in limestone/marlstone couplets from the Albian-Cenomanian Cismon section (Venetian region, northern Italy) : assessing REE sensitivity to environmental changes: Chemical Geology, v. 141, p. 141-152, doi: 10.1016/S0009-2541(97)00058-2.

Burke, K., Ashwal, L. D., and Webb, S. J., 2003, New way to map old sutures using deformed alkaline rocks and carbonatites: Geology, v. 31, p. 391-394.

Chen, L., Liu, Y. S., Hu, Z. C., Gao, S., Zong, K. Q., and Chen, H. H., 2011, Accurate determinations of fifty-four major and trace elements in carbonate by LA-ICP-MS using normalization strategy of bulk components as 100%: Chemical Geology, v. 284, p. 283-295, doi: 10.1016/j.chemgeo.2011.03.007.

Gao, S., et al., 2004, Recycling lower continental crust in the North China craton: Nature, v. 432, p. 892-897, doi: 10.1038/nature03162.

Halama, R., McDonough, W. F., Rudnick, R. L., and Bell, K., 2008, Tracking the lithium isotopic evolution of the mantle using carbonatites: Earth and Planetary Science Letters, v. 265, p. 726-742, doi: 10.1016/j.epsl.2007.11.007.

Hoernle, K., Tilton, G., Le Bas, M., Duggen, S., and Garbe-Schönberg, D., 2002, Geochemistry of oceanic carbonatites compared with continental carbonatites: mantle recycling of oceanic crustal carbonate: Contributions to Mineralogy and Petrology, v. 142, p. 520-542, doi: 10.1007/s004100100308.

Hou, Z. Q., Liu, Y., Tian, S. H., Yang, Z. M., and Xie, Y. L., 2015, Formation of carbonatite-related giant rare-earth-element deposits by the recycling of marine sediments: Sci Rep, v. 5, p. 10231, doi: 10.1038/srep10231.

Huang, Y. M., Hawkesworth, C. J., van Calsteren, P., and McDermott, F., 1995, Geochemical characteristics and origin of the Jacupiranga carbonatites, Brazil: Chemical Geology, v. 119, p. 79-99, doi: 10.1016/0009-2541(94)00093-N.

Jin, Z. J., Zhu, D. Y., Hu, W. X., Zhang, X. F., Zhang, J. T., and Song, Y. C., 2009, Mesogenetic dissolution of the middle Ordovician limestone in the Tahe oilfield of Tarim basin, NW China: Marine and Petroleum Geology, v. 26, p. 753-763, doi: 10.1016/j.marpetgeo.2008.08.005.

Jolis, E. M., Freda, C., Troll, V. R., Deegan, F. M., Blythe, L. S., McLeod, C. L., and Davidson, J. P., 2013, Experimental simulation of magma–carbonate interaction beneath Mt. Vesuvius, Italy:

Contributions to Mineralogy and Petrology, v. 166, p. 1335-1353, doi: 10.1007/s00410-013-0931-0.

Keto, L. S., and Jacobsen, S. B., 1988, Nd isotopic variations of Phanerozoic paleoceans: Earth and Planetary Science Letters, v. 90, p. 395-410, doi: 10.1016/0012-821X(88)90138-0.

Klein, C., and Beukes, N. J., 1989, Geochemistry and sedimentology of a facies transition from limestone to iron-formation deposition in the early Proterozoic Transvaal Supergroup, South Africa.: Economic Geology, v. 84, p. 1733-1774.

Liu, Y. S., Gao, S., Lee, C.-T. A., Hu, S. H., Liu, X. M., and Yuan, H. L., 2005, Melt–peridotite interactions: Links between garnet pyroxenite and high-Mg# signature of continental crust: Earth and Planetary Science Letters, v. 234, p. 39-57, doi: 10.1016/j.epsl.2005.02.034.

Liu, Y. S., He, D. T., Gao, C. G., Foley, S. F., Gao, S., Hu, Z. C., Zong, K. Q., and Chen, H. H., 2015, First direct evidence of sedimentary carbonate recycling in subduction-related xenoliths: Scientific Reports, v. 5, p. 11547, doi: 10.1038/srep11547.

Liu, Y. S., Zong, K. Q., Kelemen, P. B., and Gao, S., 2008a, Geochemistry and magmatic history of eclogites and ultramafic rocks from the Chinese continental scientific drill hole: Subduction and ultrahigh-pressure metamorphism of lower crustal cumulates: Chemical Geology, v. 247, p. 133-153, doi: 10.1016/j.chemgeo.2007.10.016.

Liu, Y. S., Hu, Z. C., Gao, S., Guenther, D., Xu, J., Gao, C. G., and Chen, H. H., 2008b, In situ analysis of major and trace elements of anhydrous minerals by LA-ICP-MS without applying an internal standard: Chemical Geology, v. 257, p. 34-43, doi: 10.1016/j.chemgeo.2008.08.004.

Mitchell, R. H., 2005, Carbonatites and carbonatites and carbonatites.: The Canadian Mineralogist, v. 43, p. 2049-2068, doi: 10.2113/gscanmin.43.6.2049.

Mourao, C., Mata, J., Doucelance, R., Madeira, J., da Silveira, A. B., Silva, L. C., and Moreira, M., 2010, Quaternary extrusive calciocarbonatite volcanism on Brava Island (Cape Verde): A nephelinite-carbonatite immiscibility product: Journal of African Earth Sciences, v. 56, p. 59-74, doi: 10.1016/j.jafrearsci.2009.06.003.

Rudnick, R. L., Gao, S., Ling, W. L., Liu, Y. S., and McDonough, W. F., 2004, Petrology and geochemistry of spinel peridotite xenoliths from Hannuoba and Qixia, North China craton: Lithos, v. 77, p. 609-637, doi: 10.1016/j.lithos.2004.03.033.

Song, Y., Frey, F. A., and Zhi, X., 1990, Isotopic characteristics of Hannuoba basalts, eastern China: Implications for their petrogenesis and the composition of subcontinental mantle: Chemical Geology, v. 88, p. 35-52, doi: 10.1016/0009-2541(90)90102-D.

Tanaka, K., Miura, N., Asahara, Y., and Kawabe, I., 2003, Rare earth element and strontium isotopic study of seamount-type limestones in Mesozoic accretionary complex of Southern Chichibu Terrane, central Japan: Implication for incorporation process of seawater REE into limestones: Geochemical Journal, v. 37, p. 163-180.

Tsikos, H., Moore, J. M., and Harris, C., 2001, Geochemistry of the Palæoproterozoic Mooidraai Formation: Fe-rich limestone as end member of iron formation deposition, Kalahari Manganese Field, Transvaal Supergroup, South Africa: Journal of African Earth Sciences, v. 32, p. 19-27, doi: 10.1016/S0899-5362(01)90016-8.

Veizer, J., 1985, Carbonates and Ancient Oceans: Isotopic and Chemical Record on Time Scales of 107–109 Years, The Carbon Cycle and Atmospheric CO2: Natural Variations Archean to Present, American Geophysical Union, p. 595-601.

Veizer, J., et al., 1999, $^{87}Sr/^{86}Sr$, $\delta^{13}C$ and $\delta^{18}O$ evolution of Phanerozoic seawater: Chemical Geology, v.

161, p. 59-88, doi: 10.1016/S0009-2541(99)00081-9.

Wells, P. R. A., 1977, Pyroxene thermometry in simple and complex systems: Contributions to Mineralogy and Petrology, v. 62, p. 129-139, doi: 10.1007/bf00372872.

Xu, R., Liu, Y. S., Tong, X. R., Hu, Z. C., Zong, K. Q., and Gao, S., 2013, In-situ trace elements and Li and Sr isotopes in peridotite xenoliths from Kuandian, North China Craton: Insights into Pacific slab subduction-related mantle modification: Chemical Geology, v. 354, p. 107-123, doi: 10.1016/j.chemgeo.2013.06.022.

Xu, Y. G., 2002, Evidence for crustal components in the mantle and constraints on crustal recycling mechanisms: pyroxenite xenoliths from Hannuoba, North China: Chemical Geology, v. 182, p. 301-322, doi: 10.1016/S0009-2541(01)00300-X.

Yan, G. H., Mu, B. L., Zeng, Y. S., Cai, J. H., Ren, K. X., and Li, F. T., 2007, Igneous Carbonatites in North China Craton: The Temporal and Spatial Distribution, Sr and Nd Isotopic Charateristics and Their Geological Significance (in Chinese with English abstract): Geological Journal of China Universities, v. 13, p. 463-473.